Characterizing groundwater recharge sources using water stable isotopes in the North Basin of Lake Kivu, East Africa

Charles M. Balagizi[1,2,3*], Marcellin M. Kasereka[1], Albert M. Kyambikwa[1], Emilio Cuoco[4], Ilenia Arienzo[4], and Marcello Liotta[3]

[1]Geochemistry and Environmental Department, Goma Volcano Observatory, 142, Av. du Rond point, Goma, Democratic Republic of the Congo

[2]Department of Chemistry, Institut Supérieur Pédagogique de Bukavu, PO Box 854, Bukavu, Democratic Republic of the Congo

[3]Istituto Nazionale di Geofisica e Vulcanologia, Sezione di Palermo, Via Ugo La Malfa, 153, 90146 Palermo, Italy

[5]Istituto Nazionale di Geofisica e Vulcanologia (INGV), Osservatorio Vesuviano, Via Diocleziano 328, 80124 Napoli, Italy

[*]Corresponding author (Charles M. Balagizi): balagizi.charles@gmail.com; +243975803568

Abstract

The $\delta^{18}O$ and $\delta^{2}H$ of rivers and springs were investigated in order to characterize the groundwater recharge sources around Nyiragongo and Nyamulagira volcanoes, in the Democratic Republic of the Congo and Rwanda. Water samples were collected monthly between

November 2013 and October 2014 from 5 major rivers, 3 major cold springs, 3 tepid springs and 1 hot spring. The temperatures of each spring were nearly constant over the sampling period attesting for their groundwater character, while the temperatures of the rivers were much more variable. The rivers monthly δ^2H and $\delta^{18}O$ range from -6.8 ‰ to 1.9 ‰ and -3.1 ‰ to 1.6 ‰, respectively, while springs showed depleted values that span from -10.2 to -1.1 ‰ for δ^2H and -3.6 to -1.9 ‰ for $\delta^{18}O$. Catchment morphology (formed of depression, upper footslope and medium to high gradient-mountains) and the local tectonic discontinuity (fissures and faults) regulate the surface runoff and subsurface flow, control the precipitation infiltration zones and hence the aquifers recharge areas. Chemical and isotopic ($\delta^{18}O$ and δ^2H) compositions of springs and rivers reveal the presence of shallow and deep aquifers, with some waters having intermediate isotope composition. Three different recharge characterized by different altitudes were identified: the first is found at low altitude ranging from ~ 1800 m to ~ 2150 m, the second and intermediate recharge zone in the altitude range from ~ 2180 m to ~ 2500 m at the upper footslope area, while the third and highest recharge area is located in the altitudes range from ~ 2620 to ~ 3220 m.. The two upper recharge areas are the most fractured and fissured zones allowing rapid infiltration of depleted precipitations which recharge deep aquifers found in the tepid and hot springs. Based on their chemical and isotopic composition waters from the shallow and deep aquifers have been considered representative of mixing end members. During their ascent to the surface, water from the deep aquifer mixes with that of shallow aquifer yielding the tepid springs of intermediate chemical and isotopic composition, while the other keep their original fingerprint corresponding to the isotopically depleted hot spring.

Keywords:

- Virunga water stable isotopes

- Groundwater recharge source
- Lake Kivu
- Virunga rivers and springs
- Nyiragongo and Nyamulagira volcanoes

1. Introduction

The water stable isotope ratios ($\delta^{18}O$ and $\delta^{2}H$) are conservative tracers suitable for characterizing the water origin and its circulation, including groundwater recharge source (Craig, 1961; Gat, 1996). Compared to the recharge precipitation, the $\delta^{18}O$ and $\delta^{2}H$ values of surface and groundwater are in fact subject to significant variation only when important evaporation of surface and soil waters have occurred, or in case the infiltrating water mixes with groundwater of different isotope composition. Therefore, their use represents an effective approach for investigating spatiotemporal groundwater recharge and post recharge processes.

The $\delta^{18}O$ and $\delta^{2}H$ of rivers are thus regarded to as the averaged weighed isotopic composition from each source feeding the river, namely runoff and groundwater. On the other hand, shallow groundwater reflects the $\delta^{18}O$ and $\delta^{2}H$ of local average precipitation, and are mostly recharged during major storm events (Holland and Turekian, 2010). However, some deep groundwater can be very old, often having been recharged thousands of years in the past (Merkel and Planer-Friedrich, 2002; Geyh, 2005). Despite their long residence time, deep groundwater conserves the $\delta^{18}O$ and $\delta^{2}H$ footprint of precipitations that recharged the aquifer (Holland and Turekian, 2010). If the stable isotope composition of precipitation changes over time, it can be used to distinguish modern and old groundwater. Indeed, Rozanski (1985) showed that European groundwaters recharged during the last glaciation period were depleted both in deuterium and in oxygen compared to modern infiltration waters.

Tectonically active zones are characterized by the presence of thin to large fractures varying from shallow to deep, in addition to faults acting as high-rate water infiltrating sites. Furthermore, these sites or the neighboring often serve as resurgence gate for hot springs or important hydrothermal activities. The latter features are associated with the fact that, in

fractured zones, the meteoric water easily infiltrates and may reach the crust where it encounters hot rocks at depth, which in some cases leads to vigorous evaporation, resulting in the enrichment in $\delta^{18}O$ and $\delta^{2}H$ of the residual waters (Craig, 1963). Thus, the $\delta^{18}O$ and $\delta^{2}H$ of hydrothermal fluids and fumaroles show significant deviation from that of corresponding local meteoric water, shifting toward enriched values (Prasetio et al., 2010; Purnomo and Pichler, 2014; Fisher and Chiodini, 2015). The groundwater residence time of such fractured zones may generally be low, ranging from hours to few decades because of the high-water infiltration and circulation rates.

The purpose of the present study is to determine the $\delta^{18}O$ and $\delta^{2}H$ of major rivers and major cold, tepid and hot springs in the fields of Nyiragongo and Nyamulagira volcanoes and the surroundings, northern basin of Lake Kivu in East Africa (Fig. 1). These springs and mountainous rivers are fed by groundwater especially during recession times (Balagizi et al., 2015). The obtained $\delta^{18}O$ and $\delta^{2}H$ of rivers and springs, in conjunction with those of precipitations (Balagizi et al., 2018a), allow characterizing the groundwater recharge sources and pathways in the north catchment of Lake Kivu. The reported dataset represents an important information for water resources management in the Lake Kivu basin, and contribute along with other dataset for future production of an improved model of the mixing processes in this lake. Moreover, the knowledge of the groundwater recharge sources in the study area is indispensable for identifying the groundwater availability and vulnerability, as springs and rivers represent the water source for the populations including for drinking, mostly used as raw. In the study area, the ongoing volcanic activity and uncontrolled development of small to major cities, as well as the increasing agricultural activities caused by a high population growth rate, might in fact yield groundwater contamination.

2. Geological, hydrogeological and climatic background

Lake Kivu is located in the western branch of the East African Rift, characterized with high tectonic and volcanic activities that yielded two major ground deformation features. The first consists of a series of mainly N-S oriented active faults related to the rift opening (Villeneuve, 1980; Coppola et al., 2016; Pouclet and Bram, 2021), with most faults being not visible on the surface (Ebinger, 1989; Balagizi et al., 2018b). The second is associated to the recent and old volcanic activity that yielded fissures and intermediate to wide fractures (Fig 1 and Fig. 2), as a consequence of repetitive magma intrusions (Komorowski et al., 2004; Balagizi et al., 2016), some fractures extending beneath Lake Kivu (Villeneuve, 1980; Wauthier et al., 2012; Balagizi et al., 2020). The Mitumba range (~3000 m a.s.l.) and the Rwandan dorsal (~ 2850 m a.s.l.) form walls respectively to the West and East of the rift (Fig. 1).

The lithology of the northern area of Lake Kivu basin consists of a Precambrian formation basement (metamorphic rocks to the West, quartzite and schist to the South-East) and igneous basalts occurring in the volcanic field (Fig 2A) with both active and dormant volcanoes. Lavas in the study area are from Nyiragongo, Nyamulagira and Karisimbi volcanoes belonging to the western and central part of the Virunga Volcanic Province (Fig 2A). Nyiragongo lavas are highly alkaline and strongly silica-undersaturated, Nyamulagira lavas are compositionally less extreme (Aoki et al., 1985; Platz et al., 2004, Head et al., 2011, Balagizi, 2016), these two volcanoes are the presently active of the Virunga while Karisimbi lavas have been dated at 0.010 ± 0.007 Ma (De Mulder and Pasteels, 1986). Several monogenic cones are observed in the volcanic field (Fig 2A), and are composed of pyroclastic deposits whereas the lava flows show a succession of pahoehoe and aa lavas, with scoria being present at some places even though less dominant.

Combined topography (Fig 1) and slope (supporting information Fig. S1) reveal three main types of landforms that include depression, upper footslope and medium to high gradient-mountains, which imply three main hydrogeological zones of the terrain (Fig. 2B). The depression corresponds to the flat large lava field plain and other low-lying lands along the vicinity of Lake Kivu shores, some of the latter are depositions from the eroded soil from the hills and Mitumba mountains (Fig 2A & 2B). The upper footslope area is found in the mid-segment of the mountains (e.g. at Nyiragongo as well as at the mountains of the Rwandan dorsal) and has gentle to steep slopes, while the medium to high gradient mountain zone corresponds to the steeper segments of the mountains. They are found at the summit area of Nyiragongo volcano, at the highest segment of the Mitumba mountains and the Rwandan dorsal (Fig 2B). Cavities and tunnels are present at some places of the two lowest zones in the volcanic field (i.e. depression and upper footslope), and serve as channel for underground water flow. The soil formed from acid metamorphic parent materials to the West (Kingi site and the area from Minova to part of Sake), while Goma, Gisenyi, Kanyaruchinya, Kibati and the other part of Sake are formed of ancient to recent lava flows (Fig. 2A). Further descriptions of the dominant soil types, as well as the land use and cover in the study area can be found in Balagizi et al. (2015).

No surface rivers drain the Nyiragongo volcanic field. Kamutoni, Mubambiro, Sake Birere and the Tingi group of springs are found to the extreme south part of Nyamulagira volcano, all discharging into the Kabuno bay (Fig. 1 and Fig. 2A). Lithology and volcanism exert strong influences on the geochemical composition of these rivers and springs, yielding high-mineralized waters in the volcanic field (e.g. high major cations and DIC) and low-mineralized in the metamorphic formation (Balagizi et al., 2015). The region undergoes typically humid tropical climate of two seasons, the rainy (September to June) and the dry (July to August), a small dry season is observed from mid-January to late February. The mean annual precipitation

ranges between 1300 and 1700 mm in the lowlands of the study area, but shows values up to 2300 mm in the highlands (Balagizi et al., 2017). The repetitive eruptions of Nyamulagira volcano and the permanent plume of Nyiragongo volcano strongly impact the rainwater chemistry and the environment (Cuoco et al., 2012 a,b; Balagizi et al., 2019; Kasereka et al., 2021). The evapotranspiration in the Lake Kivu catchment is estimated in the range of 900 and 1500 mm yr^{-1} (Muvundja et al., 2014).

3. Samples and Methods

The sampling sites are in the elevation range between Lake Kivu (1460 m a.s.l.) and the summit of Nyiragongo volcano (3470 m, Fig. 1). Monthly sampling campaigns were conducted on 5 rivers (i.e. Mubimbi, Renga, Shasha, Kihira and Sebeya) and 7 springs (Tingi 1, Tingi 2, Tingi 3, Sake Birere, Kamutoni, Mubambiro and Rambo; Fig. 1) in the north catchment of Lake Kivu. Samples were collected between November 2013 and October 2014, which covers once each of the two seasons, i.e. the wet and dry. In the rivers, samples were collected at the middle of the water column, while samples from springs were collected directly at the resurgence point. All the rivers and springs discharge into the Kabuno Bay except Mubimbi, Sebeya and Rambo that discharge in the main basin of Lake Kivu (Fig. 1). On the other hand, during the same period, rainwater samples were collected monthly from a rain-gauge network of 13 stations spreading over the study area at different altitudes (Fig. 1). The chemical composition of the rainwater has been reported in Balagizi et al. (2017), while their $\delta^{18}O$ and $\delta^{2}H$ were reported in Balagizi et al. (2018) and Balagizi and Liotta (2019). The two latter discuss the $\delta^{2}H$, $\delta^{18}O$ and deuterium excess (d-excess) spatiotemporal variations in relation to the local geomorphology and hydrology. Further, two field campaigns of water sampling were conducted on Lake Kivu, with

water collected at the surface, 5 and 10 m depth in the Kabuno Bay, and at the surface and 25 m depth in the Main basin (Fig. 1). All samples were filtered through 0.45-mm-pore-size polysulfone syringe filters in the field, and stored at room temperature in 30 mL high-density polyethylene plastic bottles with double screwcaps. No chemicals were added to the samples for the preservation. Water temperature was measured in situ with a YSI ProPlus probe in rivers and cold springs, and with a Fluke Thermocouple Thermometer 51/52 II in tepid and hot springs. The Fluke Thermocouple accuracy is 0.05% + 0.3°C and resolution of 0.1°C for temperatures below 100°C, and 0.5% + 0.3°C and resolution of 1°C for temperatures above 100 °C.

Water samples were analyzed for hydrogen and oxygen stable isotopes in the Isotope Hydrology Laboratory of the International Atomic Energy Agency (IAEA) in Vienna, by an off-axis integrated cavity output laser spectroscopy (OA-ICOS), following analytical procedure of Wassenaar et al. (2014). The typical uncertainties, reported as the long-term standard-deviation of a control sample and amounts, were of 0.50‰ for δ^2H and 0.08‰ for $\delta^{18}O$, further analytical details are given in Balagizi at al. (2018a). The d-excess was deduced from $\delta^{18}O$ and δ^2H using the relation $d=\delta^2H-8\delta^{18}O$ after Dansgaard, 1964. The δ^2H and $\delta^{18}O$ mean precipitation-weighted values (δ_{pw}) were calculated according to:

$$\delta_{pw} = \frac{\sum_{i=1}^{n} \delta_i \, x \, P_i}{\sum_{i=1}^{n} P_i} \quad (1)$$

where δ_i is the measured monthly δ^2H or $\delta^{18}O$ value for the i-th month and Pi is the monthly precipitation for the i-th month.

4. Results and Discussion

4.1. Temperature and isotopic composition of springs and rivers

198

199 The minimum, arithmetic mean and maximum temperature, precipitation, δ^2H, $\delta^{18}O$ and
200 d-excess of rivers and springs waters are reported in Table 1, the full dataset is given in Dataset 1
201 supplementary material. Cold springs showed the lowest temperatures, which can be assimilated
202 to that of local groundwater, as the samples were collected at the resurgence points. Their mean
203 temperatures were in the range of 17.4 °C (Kamutoni and Mubambiro) and 21.7 °C (Tingi 3) and
204 were almost constant over the sampling period. The difference between the highest and lowest
205 temperature values (ΔT) for each cold spring was < 0.3°C. Rivers temperatures are generally
206 higher than that of cold springs (Table 1). However, some rivers showed low temperatures, e.g.
207 mean of 18.8 °C in Mubimbi, 20.6 °C in Kihira and 21.9 °C in Renga, in line with their high
208 altitude origin in the Mitumba mountains (Fig. 1 and Fig. 2). During the sampling period, the ΔT
209 in rivers was higher than that observed for cold springs with ΔT of up to 5.8 °C for Shasha. The
210 tepid (temperature up to 29.5°C) and hot (temperature up to 73.2°C) springs also had almost
211 constant temperature, with ΔT < 1 °C for each. The tepid springs showed a mean temperature of
212 26.6 °C for Tingi 1 and 29.3 °C for Tingi 2 which are at least 4,0 °C above the local mean annual
213 air temperature at lowest (21.0 °C) and highest altitudes (9.6 °C) (Balagizi et al., 2015, 2017).
214 The mean yearly precipitation at spring and river sampling sites are close because of their
215 location at similar altitudes in the local lowland based on a classification after Balagizi et al.
216 (2017). The altitude difference between the most (Mubimbi river, 1505 m) and least (Rambo
217 Spring, 1461 m) elevated sites is in fact < 50 meters (Table 1).

218 The rivers' monthly δ^2H values range from -6.8 ‰ in Mubimbi and 1.9 ‰ in Sebeya,
219 while Shasha show the highest monthly $\delta^{18}O$ value (-1.6 ‰) and Mubimbi the lowest (-3.1 ‰).
220 Compared to rivers, springs (cold, tepid and hot included) show depleted monthly δ^2H (-10.2 to -
221 1.1 ‰) and $\delta^{18}O$ (-3.6 to -1.9 ‰) values (Table 1). The d-excess is high in tepid springs with

mean value up to 21.89 ‰, while Rambo hot spring shows values between 16.2 and 18.1 ‰. The cold springs generally show intermediate d-excess mean values, whereas the rivers are characterized with the most depleted mean d-excess going down to 13.5 ‰ in Shasha river.

4.2. Spatial variations of isotopic composition

The monthly δ^2H and $\delta^{18}O$ of springs and rivers are similar except for Tingi 1 and Rambo which are warm and hot springs respectively, and that have values shifting towards depleted $\delta^{18}O$ values; Rambo further shows the most depleted δ^2H (Fig. 3A). However, the monthly δ^2H and $\delta^{18}O$ of springs and rivers are all included in the range of mean precipitation-weighed values of the local rainwater (-11.7 to 5.5‰ for δ^2H, and -4.0 to -1.1 ‰ for $\delta^{18}O$, Fig. 3B and Table 2). Such an enclosure indicates that springs and rivers were fed by recent local groundwaters which in turn are recharged by recent local rainwater, in opposition to possible contribution from regional and/or old groundwaters of different isotope composition. The cold springs, i.e. Mubambiro, Kamutoni, Sake Birere and Tingi 3, have isotopic composition close to that of rivers (most enriched, Fig. 3A, Table 1), as a consequence of the similarity in the isotope composition of the lowland rainwater (Table 2) that predominantly recharge their systems. On the contrary, Rambo hot spring, Tingi 1 and Tingi 2 tepid springs are fed by a different system, which has isotopic composition similar to that of depleted highland rainwater (Fig. 3B and Table 2). Tingi 1, Tingi 2, Tingi 3 and Sake Birere are springs located few hundred meters apart; Mubambiro and Kamutoni springs are spatially close one another and both located about 3 km away from the Tingi group (Fig. 1 & 2). The two groups of springs are fed by both deep and shallow aquifers, with Tingi 1 being compositionally closer to the parental deeper end member that is in contact with the hot bedrock and Tingi 3 closer to the upper shallow end member.

The blue solid line of Fig. 3C represents the linear best fit of all the datapoints, i.e. of mean δ^2H and $\delta^{18}O$ of rivers and springs. The equation is $\delta^2H = 4.5\delta^{18}O + 6.1$ ($R^2 = 0.71$; $p < 0.0001$) and divides the corresponding 99 % confidence interval zone into two parts. The upper part contains the mean values of springs which are aligned along the grey line. This latter corresponds to a mixing line between a deep and a shallow groundwater reservoir, with Tingi 1 spring and Shasha river appearing as mixing end members. This grey line almost coincides with the linear best-fit line of springs datapoints taken separately, and is described by the equation $\delta^2H = 4.8\delta^{18}O + 7.9$ ($R^2 = 0.86$, $p < 0.01$; Fig. 3C). During its ascent to the surface the deep and hot water end member progressively mixes with cold water from the shallow aquifer yielding compositionally intermediate waters of relatively low temperature but with enriched isotopic signature. At the resurgence points, the mean temperatures of Tingi 1, Tingi 2, Tingi 3, Sake Birere, Kamutoni and Mubambiro are 29.3, 26.6, 21.7, 18.2, 17.4, and 17.4°C, respectively (Table 1). The observed trend of decreasing in springs temperatures, along the mixing path from deep to shallow aquifers (Table 1), points out the evidence that Tingi 3, although spatially close to the other Tingi springs, is more affected by water from the upper aquifer than Tingi 2 or Tingi 1. Similarly, Sake Birere, Kamutoni and Mubambiro rivers are much related to the upper aquifer. This mixing path between the upper and deep aquifers is in line with both the observed progressive δ^2H and $\delta^{18}O$ enrichment in springs, and their simultaneous decreasing in temperatures. As the hot depleted deep-waters ascent towards the surface, they progressively mix with cold and isotopically enriched shallow water. Once at the surface, water from the shallow aquifer becomes dominant, the resulting mixture yields temperature and isotopic signature closer to that of shallow aquifer (e.g. Tingi 3; Fig. 3A&C), i.e. of cold springs such as Sake Birere, Kamutoni or Mubambiro.

The mixing hypothesis is further supported by the chemical composition of springs, with Tingi 1 showing the highest values of TDS and total alkalinity (TA) with respect to Tingi 2 and Tingi 3. The TDS are in the order of 3115.09 mg L^{-1}, 2184.83 mg L^{-1} and 794.53 mg L^{-1} for Tingi 1, Tingi 2 and Tingi 3, respectively, while the TA are 2685.65 mg L^{-1}, 2419.11 mg L^{-1} and 657.69 mg L^{-1} for Tingi 1, Tingi 2 and Tingi 3, respectively (Balagizi, 2016). The chemistry of water from Tingi 3 is similar to that of Sake Birere, Kamutoni and Mubambiro that have TDS values of 864.0 mg L^{-1}, 811.7 mg L^{-1}, 821.6 mg L^{-1} and TA of 802.94 mg L^{-1}, 692.11 mg L^{-1} and 689.17 mg L^{-1} respectively (Balagizi, 2016).

Rambo is another deep end member located to the eastern part of the study area far from the Tingi group (Fig. 1) and with a different ascending path (Fig. 3C). In Figures 3C and 3D it is aligned with Mubimbi and Renga rivers even if they are located to the western part of the study area. Rambo hot spring is located on the shoreline of Lake Kivu; however, it seems there are no intrusions of the lake water into the ascending hot spring water. In fact, Rambo's δ^2H and $\delta^{18}O$ mean values (-9.5‰ and -3.3 ‰, respectively; Table 1) are very depleted compared to both Lake Kivu surface water (δ^2H= 27.0 ‰, $\delta^{18}O$ = 3.5 ‰) and water from 25 m depth (δ^2H= 26.7 ‰, $\delta^{18}O$ = 3.6 ‰; Table 2) such that any mixing with the lake waters during the ascent is excluded. The lowest part of the confidence interval zone of Fig. 3C contains only the mean values of rivers, which are in-between Shasha river and Rambo hot spring that appear as the two end members. Contrary to the springs, the rivers datapoints (Mubimbi, Renga, Sebeya and Shasha) are aligned along the green line that corresponds to the evaporation line of equation $\delta^2H = 4.83\delta^{18}O + 7.89$ ($R^2 = 0.86$; $p < 0.01$). Kihira is the only river that is situated above the blue linear best fit. Such position was expected for Kihira, as this river is formed of two tributaries: the first is formed of waters from the Tingi group-Sake Birere springs which mixes with another small river that originates from the Mitumba range. Kihira samples were collected downstream

293 the mixing point which causes its δ^2H and $\delta^{18}O$ values shift towards springs values. In fact,
294 during recession periods, the water from the Tingi group-Sake Birere springs predominates,
295 which is the frequent case because the Mitumba river flow quickly decreases few days after the
296 last rains (see more in Balagizi et al., 2015). On the other hand, with 72.7°C of mean
297 temperature, Rambo surface water appears as the most depleted end member compared to rivers,
298 along the defined evaporation line (Fig. 3D). Even though Rambo and the rivers undergo a
299 similar or close process that cause such an alignment, they have different chemical composition
300 discussed in Balagizi et al. (2015) and Balagizi, 2016; with Rambo being highly mineralized
301 (TDS= 1958.10 mg L^{-1}, Balagizi et al., 2016) compared to the rivers (e.g. the TDS value is
302 372.33 mg L^{-1} for Shasha, 168.69 mg L^{-1} for Renga, 81.20 mg L^{-1} for Mubimbi and 74.7 mg L^{-1}
303 Sebeya; Balagizi et al., 2015). The rivers may undergo limited evaporation in the course of the
304 flow: the most evaporated and hence highly enriched end member being Lake Kivu surface
305 waters (Table 2) which they feed.

306 The two known deep end members, i.e. Rambo and Tingi 1, are both recharged by the
307 local highland rainwater (see section 4.5). Once the rainwater has entered the groundwater
308 system, an exchange between the infiltrating water and the aquifer occurs, e.g. mixing and
309 water–rock interaction, as well as possible evaporation at depth, in correspondence of the contact
310 with the hot bed rock. These interactions are known to produce variations in the isotope signature
311 of the water (Huang and Pang. 2012; Liu et al., 2016). The degree of such variations depends on
312 the chemical composition of the rocks, on the aquifer temperature, and on the groundwater
313 residence time (Yin et al. 2001). A very slight difference exists between the $\delta^{18}O$ in Rambo and
314 Tingi 1 (Fig. 3A and Table 1), which may be related to the difference in the lithology and the
315 temperature between the two systems (Fig. 2A). The water–rock interaction rates in the systems
316 feeding Rambo and Tingi 1 are possibly different due to the difference in the temperature

between the systems (e.g. Mironenko and Zolotov, 2012). However, the difference of interaction rates cannot alone yield such a significant shift in the $\delta^{18}O$ between the two systems. Looking at their $\delta^{2}H$, there is a more significant difference in the $\delta^{2}H$ values of the two deep end members, with Rambo shifting towards depleted $\delta^{2}H$ values (Fig. 3C), and consequently yielding a decrease in its d-excess compared to that of Tingi 1 (Fig. 3D). The decreasing in both the $\delta^{2}H$ and the d-excess in Rambo could likely results from a stronger evaporation (due to high temperature) occurring under kinetic fractionation (due to high ascent velocity of the condensate) compared to Tingi 1. Further, during their ascent the deep end member in the area of the Tingi group mixes with shallow groundwater which likely reduces the effect of any possible evaporation that occurs at depth. On the contrary, Rambo water does not mix with water of the nearby Lake Kivu, as attested by the fact Rambo datapoints plot on the Local Meteoric Water Line (Fig. 3C). The effects of the evaporation at depth (formation of depleted vapor) and the kinetic fractionation during the ascent are conserved and result in the observed decrease in the d-excess in Rambo (Fig. 3D).

Overall, the above groundwaters classification into two end members based on their $\delta^{18}O$ $\delta^{2}H$ values, i.e. Tingi 1 and Rambo on one side, and Sake Birere, Mubambiro and Kamutoni on the other, is in line with the already mentioned mineralization trend, but is additionally supported by chlorine data. In fact, the hot and deep end members contain higher chloride concentrations, Tingi 1 and Rambo contain between 6 and 13 times more chloride compared to the shallow springs (Balagizi et al. 2016). Some other tracers such as B, Li, and Si follow a similar trend, with concentrations in deep aquifers, represented by the Rambo and Tingi 1 springs, being 71.5 to 3238.5 times for Li, 16.7 to 60.6 times for B and 0.9 to 1.7 times for Si higher than that in the shallow aquifers (Sake Birere, Kamtoni and Mubambiro cold springs) (Balagizi, 2016). These

trends are in agreement with the descriptions by Marini (2004) regarding trace elements ratios between geothermal waters circulating in deep aquifers and cold waters of shallow aquifers.

4.3. Temporal variations of isotopic composition of rivers and springs

The δ^2H, $\delta^{18}O$ and d-excess temporal evolution of springs and rivers did not show any well-defined seasonal variation (Fig. 4), contrary to the well-pronounced seasonality observed in Virunga rainwaters (Balagizi et al. 2018a), in eastern African precipitations (e.g. IAEA/WMO, 2017; Munyaneza et al., 2012; Levin et al., 2009; Mduma et al., 2016), and in global precipitations (e.g. Hoefs, 2009; Gat, 2010; Pfahl and Sodemann, 2014). Some rivers, particularly Shasha and Renga, showed a slight increase of δ^2H and $\delta^{18}O$ during the January-February short dry season (Fig. 4A&B) as a consequence of the isotopic composition enrichment of precipitation in this period (see discussion in Balagizi et al., 2018a). Furthermore, the δ^2H values of rivers were more sensitive to this slight increase (Fig. 4A) compared to that of $\delta^{18}O$ (Fig. 4B), because of the kinetic fractionation that mostly impacts light molecules. On the other hand, no notable increase in the rivers δ^2H and $\delta^{18}O$ were observed during the July-August major dry season (Fig. 4A&B) despite the important decrease in the precipitation amounts (Fig. 5), which partly resulted in the δ^2H and $\delta^{18}O$ enrichment of Virunga rainwater (Balagizi et al., 2018a). The high isotope enrichment of Virunga precipitations during the main dry season was not observed in rivers mainly because the rain amount was very low: 7.5 to 13 mm/month in July and August, compared to values up to 320 mm/month in December at the same lowland station (Fig. 5). Because the soil is very dry in this period (Zomer et al. 2007, 2008; Trabucco and Zomer, 2009), the 7.5-13 mm/month could not cross the unsaturated zone or significantly change

363 the isotope composition of river water. Similarly, springs did not show any well-defined δ^2H and
364 $\delta^{18}O$ variations that may be linked to season changes (Fig. 4D, E&F).

365 Virunga rainwaters showed very large change of isotope composition as a consequence of
366 season variation (e.g., from -18.5 to 56.0 ‰ for δ^2H, -4.6 to 6.2 ‰ for $\delta^{18}O$ and 6.7 to 22.0 ‰, at
367 Kanyaruchinya lowland site, Table 2), a strong seasonality which was not simultaneously
368 observed in springs and rivers of the north basin of Lake Kivu. Such a lack of simultaneity in the
369 δ^2H and $\delta^{18}O$ temporal evolution in rainwater, springs and rivers is due to the already mentioned
370 precipitation amounts decrease, which could not reach the aquifer during the dry season. For the
371 remaining periods of the year, which are principally rainy (Fig. 5), it is due to the tectonic
372 discontinuity, the volcanic fissures as well as the drainage basin lithology and morphology (Fig.
373 2A&B) that control the rainwater infiltration, the surface, near surface and underground flows. In
374 fact, the tectonic discontinuity and the fissures are places for rapid water infiltration which
375 prevent the formation of surface flows and runoff that may directly reach the rivers. In the areas
376 without faults and fissures, the landform controls the rainwater infiltration rate and runoff
377 formation and rate. Thus, the two upper landforms, i.e. the upper footslope and the medium to
378 high gradient-mountains (Fig. 2B), are steep zones (supporting information Fig. S1) that
379 generates high surface flows velocities, and are thus zones with limited infiltration. As a result,
380 surface flows and runoff water quickly reach the rivers causing immediate increase in the river
381 flow (flooding). However, this increase finishes within the few hours following the end of the
382 rain events in this mountainous catchment. This rapid surface runoff and subsurface flow run out
383 yield very short rainwater residence time in the soil. Consequently, the rivers and springs water
384 are most of time composed of homogenized water from the aquifer (i.e., of nearly constant
385 isotope composition), unless the rivers or springs are sampled a few hours following a rain event.
386 However, the small amount of rainwater that remains in the soil undergoes evaporative-

387 enrichment but can't reach the river channel through lateral subsurface flow. This slightly
388 enriched water may reach the aquifers either by infiltration, or being transported by the water
389 infiltrating during the following rain events. The infiltrating soil-enriched water mixes with
390 water in the aquifer, but its impact on the final isotopic composition of mixed groundwater
391 depends on the amount of each component (e.g. Kendall, 1993; DeWalle and Swistock, 1994).
392 On the other hand, rain that falls in the zone of very low slope, shown as the depression in the
393 landforms map of Fig. 2B may undergo more isotope enrichment during the infiltration
394 compared to that of the two upper landforms of higher slopes. Still, in some areas particularly in
395 the field of Nyiragongo and Nyamulagira volcanoes, the presence of fissures and pyroclastic
396 deposits cause very high infiltration rates, which further limits evaporation during the infiltration.
397 Although the isotopic composition of the springs and rivers is not strongly altered by the
398 evaporation, it is observed that, with the exception of very few data points, the monthly δ^2H and
399 $\delta^{18}O$ of rivers and some springs plot below the Local Meteoric Water Line (LMWL) (Fig. 3A).
400 This is indicative of the weak evaporation occurring during the water infiltration that yields weak
401 isotope enrichment, especially in catchments with relatively small plain or gentle slope (e.g.
402 Sebeya, Renga and Shasha). This evaporation was not seasonal-strictly dependent as the local
403 temperature and relative humidity are nearly constant on daily basis, have values that can yield
404 important evaporation throughout the year. In fact, the daily minimum and maximum
405 temperature of ~ 13.5 °C and 29.5 °C, respectively, and the 70 – 84 % of monthly relative
406 humidity where recorded both in the rainy and dry seasons (Fig. 5). The infiltration of slightly
407 enriched evaporated water is favored by plain and/or gentle slope since they generate slow
408 surface and subsurface lateral flows, which increases soil rainwater residence time. In addition,
409 some of these catchments receive enriched lowland rainwaters (undergoes enrichment during the
410 fall or formed from the condensation of strictly local recycled enriched moisture; see discussion

411 in Balagizi et al., 2018). Any weak evaporation of this water during the infiltration could yield
412 water with noticeable offset compared to the LMWL, which also distinguished them from that of
413 Tingi 1 and Rambo (Fig. 3A) that are recharged by highland rains (see previous discussion and
414 that in section 4.5).

415 In bimodal seasons, the contribution from each source to the river discharge changes with
416 the season, with precipitation dominating in rainy season and groundwater during base flow
417 conditions in the dry season. The influence of precipitation decreases as rains become scarce,
418 while on the other hand that from subsurface flows and groundwater rises. Because of the
419 evaporation of soil water, the residual soil water shows ^{18}O and ^{2}H enrichment, which influences
420 the isotopic composition of the next groundwater recharge and subsurface runoff. However, the
421 extent of the influence depends on both the amounts of the residual soil water and of the
422 precipitation that mix. Thus, it has been observed that rivers of small catchments respond faster
423 to changes in the ^{18}O and ^{2}H of precipitations, leading to well pronounced and correlated
424 seasonality in both rivers and rain (e.g. Dewalle et al., 1997; Genereux and Hooper, 1998).

425

426 **4.4. Oxygen isotope – precipitation, air temperature and relative humidity dependency**

427

428 As for the $\delta^{18}O$ precipitation weighted values, the monthly precipitation $\delta^{18}O$ of rivers
429 and springs also reveal that isotope composition of surface and groundwater is weakly impacted
430 by monthly precipitation variation (Fig.6A). This is related to the fact that the isotopically
431 enriched rainwater of the dry season (Balagizi et al. 2018a) does not reach the aquifer because
432 soil is very dry and rain vents are very scarce during this period (Fig. 5). On the other hand,
433 during the major rain season (e.g., October to December and March to early May, Fig. 5) the
434 falling rain generate very high flows in the rivers because of the high slope of this mountainous

region (Balagizi et al., 2015). The flow rate drastically decreases a few hours after a rain event, leaving small amount of water in the soil, which cannot impact the isotope composition of rivers, because the latter is dominated by water from the springs. The infiltration mainly takes place at high rates because of the lithology and morphology in the study area (Fig. 2A&B), i.e. prevalence of faults, fractures and fissures, of pyroclastic flows at same places, which are very porous conducting to high infiltration rates. This yielded the absence of correlation between monthly $\delta^{18}O$ and the precipitation (R^2= 0.03 in rivers and R^2=0.009 in springs; Fig. 5A).

Similarly, air temperature and relative humidity variations did not show any impacts on the isotopic composition of rivers and springs (Fig. 6B&C). These two parameters, along with the wind speed, control the surface and soil water evaporation. They were found to partly be responsible for the seasonality observed in Virunga rainwater because they yielded isotopically enriched moisture (formed mainly from the already enriched surface waters such as Lake Kivu, Table 2) which in turn produced enriched rainwater or enrichment of the rain drops during their fall (Balagizi et. al, 2018). However, the isotopically enriched rainwater produced during the dry season does not reach the aquifer because of their small amounts as discussed above, causing the absence of seasonality in rivers and springs. Furthermore, the daily mean temperature and the relative humidity are nearly constant during the course of the year (Fig. 5). This determines the absence of correlation between water isotope composition, temperature (R^2=0.006 for rivers and R^2= 0.0011 for spring; $p< 0.001$, Fig. 6B) and relative humidity (R^2= 0.02 for rivers and R^2=0.01 for springs, $p< 0.001$; Fig. 6C).

4.5. Groundwater meteoric water recharge area

458 The fact that springs and rivers have monthly isotope composition included in the range
459 of precipitation-weighed $\delta^{18}O$ and $\delta^{2}H$ of local rainwater is evidence that they are fed by local
460 aquifers recharged by recent precipitations, or by older water of long residence time having
461 similar stable isotope signature (Fig. 3B). The equation relating the mean precipitation-weighted
462 $\delta^{18}O$ of Virunga rainwater to the altitude ($\delta^{18}O$ (‰) = - 0.0012z + 0.2848, z is the altitude; Balagizi
463 et al., 2018a) can consequently be used to estimate the groundwater recharge area. A local
464 vertical $\delta^{18}O$ gradient line was thus obtained using this equation, which corresponds to the solid
465 black line of Fig. 7. The same equation similarly allows estimating the altitude range at which
466 meteoric waters recharging the aquifers infiltrate, by using the mean precipitation-weighted $\delta^{18}O$
467 of rivers and springs. The latter appear aligned along the local vertical $\delta^{18}O$ gradient line once
468 plotted against the corresponding computed altitudes (Fig. 7).
469 Three main areas of groundwater recharge are observed based on the altitudes computed
470 using the mean precipitation-weighted $\delta^{18}O$ values of springs and rivers, and correspond likewise
471 to the three main landforms of Fig. 2B; i.e. depression or the lava plain, upper footslope and
472 medium to high gradient-mountains. The approximate limits of these three main areas have been
473 estimated on the basis of the field analysis, i.e. the topography and geology of the study area.The
474 first area of groundwater recharge occurs in the altitude range from ~ 1800 m to ~ 2150 m and
475 feeds shallow aquifers (Fig. 7), corresponding to mean precipitation-weighted $\delta^{18}O$ from -1.88 to
476 -2.28 ‰. Such $\delta^{18}O$ range includes Shasha river, Tingi 3 and Sake Birere springs which are fed
477 by isotopically enriched water from shallow aquifers and potentially surface flows. The recharge
478 area range corresponds to the altitudes below 2150 m formed by the large plain (Fig. 2B)
479 favoring the already evoked relatively evaporative infiltration. Further, this area receives
480 isotopically enriched lowland precipitations (Balagizi et al., 2018a), which causes the $\delta^{18}O$ and
481 $\delta^{2}H$ of Shasha river departing from the general trend (Fig. 3C&D). Part of the rainwater falling

over this area directly reaches the neighboring Lake Kivu as surface runoff or superficial subsurface flows, likely without transiting through an aquifer. The case for rainwaters from Bweremana, Buhimba, Sake and OVG sites located not far from Lake Kivu shoreline (Fig. 1). The second area of groundwater recharge occurs in the altitude range from ~ 2180 m to ~ 2500 m and feeds shallow to intermediate aquifers of mean precipitation-weighted $\delta^{18}O$ from -2.3 to -2.7 ‰ (Fig. 7), corresponding to the upper footslope area of Fig. 2B. Except Shasha, all the other rivers are fed by waters recharged at these altitudes, in addition to Kamutoni and Mubambiro cold springs. The third recharge area is found in the altitudes range from ~ 2620 to ~ 3220 m, which corresponds to the high gradient-mountains zone thus including the summit area of Nyiragongo volcano and other neighboring high-altitude zones such as the Mitumba chain and the Rwandan dorsal, located respectively to the west and east of Lake Kivu (Fig. 1). Tingi 1 and 2 tepid springs as well as Rambo hot spring are fed by waters whose aquifers are recharged at these altitudes. The two upper recharge areas, i.e. upper footslope and medium to high gradient-mountains, are the most fractured and fissured zones (Fig. 1) which allow rapid infiltration of highland depleted precipitations, which recharge deep aquifers and found in the tepid and hot springs generated after being in contact with the hot bed rock.

The $\delta^{18}O$ composition of Lake Kivu water (surface down to 25 m depth, Table 2) were also added to Fig. 7 for comparison, considering the lake's altitude of 1460 m. This upper layer of the lake is fed by direct rainwater falling over the lake surface, as well as surface flows from the catchment (rivers and runoff), and which undergo intense evaporation and seasonal mixing once in the lake. In fact, a study by Muvundja et al., (2014) estimated to ~ 60% the Lake Kivu water output due to surface evaporation. This strong evaporation yields high isotopically enriched residual water of the upper layer of Lake Kivu, resulting in the shifting of the lake's $\delta^{2}H$ and $\delta^{18}O$ compared to that of rivers and rain entering this layer (Fig. 7).

5. Conclusions

We present the first time series of oxygen and hydrogen isotope composition of major rivers, cold springs, tepid springs and one hot spring in the north basin of Lake Kivu, western branch of the East African Rift system. The isotope composition of the rivers and springs allowed identifying the groundwater recharge sources in this young volcanic and tectonic filed. The main conclusions of the present study are summarized as follows:

- The landform is subdivided in three main classes that include depression, upper footslope and medium to high gradient-mountains; implying three major hydrogeological characteristics of the terrain, and corresponding to three main hydrogeological zones.

- Three main zones of groundwater recharge have been identified and correspond to the three main landforms of the terrain: the first occurs in the altitude range from ~ 1800 m to ~ 2150 m (above sea level) and feeds shallow aquifers, corresponding to aquifers of mean precipitation-weighted $\delta^{18}O$ from -1.88 to -2.28 ‰, fed by isotopically enriched precipitation from Virunga lowland. The second zone of groundwater recharge goes from the altitude of ~ 2180 m to ~ 2500 m, corresponding to the upper footslope area, and feeds shallow to intermediate aquifers of mean precipitation-weighted $\delta^{18}O$ from -2.3 to -2.7 ‰. The third recharge zone is located in the altitudes range from ~ 2620 to ~ 3220 m, corresponding to the high gradient-mountains that collect highland depleted precipitations which recharge deep aquifers, and the latter feed the tepid and hot springs.

- Combined catchment morphology, local tectonic discontinuity and to a larger extend the lithology (1) regulate the surface runoff and subsurface flow, (2) control the precipitation infiltration zones and hence the aquifers recharge areas. The steep slope generates high surface flow and runoff rates that quickly reach the rivers and yield abrupt increase in the river flow. In this mountainous catchment, the river high flow runs out within the few hours following the end of the rain events**.**

- The cold springs (temperature range from 17.40 to 21.8°C) showed each almost constant temperature over the sampling period owing to their groundwater character. Rivers temperatures (range from 17.4 to 26.9°C) varied over the sampling period, and were generally few units higher with respect to that of cold springs, with values linked to their high-altitude origin. Similarly to cold springs, tepid springs (temperature range, 26.2 - 29.5°C) and the hot spring (72.7°C) had their temperature nearly constant over the sampling period, as they varied of less than 1°C, respectively.

- The monthly δ^2H (-10.21 ‰ to 1.96 ‰) and $\delta^{18}O$ (-3.58 ‰ to -1.62 ‰) of rivers and springs are included in the range of the local monthly precipitation values (-11.66 to 5.45 ‰ for δ^2H and -4.00 to -1.07 ‰ for $\delta^{18}O$), indicating that the aquifers feeding the springs and rivers are recharged by recent local precipitations; with possible contribution of older groundwater of similar stable isotope signature.

- The δ^2H, $\delta^{18}O$ and d-excess temporal evolution of Virunga springs and rivers did not show any well-defined seasonal variation that may be linked to season changes. During the dry season, an important decrease of the precipitation amount is observed but the small amount

of rain could not cross the unsaturated zone because the soil is dry. Thus, direct precipitation has no immediate influence on the $\delta^{2}H$ and $\delta^{18}O$ values of springs and rivers in the Virunga.

Acknowledgments

Water samples were analyzed by the International Atomic Energy Agency (IAEA, Isotope Hydrology Laboratory), Vianna; within the framework of the Global Network of Isotopes in Precipitation (GNIP), and the Global Network of Isotopes in Rivers (GNIR). The authors acknowledge useful comments and recommendations from two anonymous reviewers, which improved the manuscript, and the editorial handling of Christian France-Lanord.

Author contributions

Charles M. Balagizi conceived the study and the samples collection protocol, the latter was then commented by Marcello Liotta, Marcellin M. Kasereka, Albert M. Kyambikwa and Emilio Cuoco. The field works were carried out by Marcellin M. Kasereka, Charles M. Balagizi and Albert M. Kyambikwa. Charles M. Balagizi, Ilenia Arianzo and Marcello Liotta analysed and interpreted the data. Charles M. Balagizi drafted the manuscript which was latter considerably commented, mended it for important intellectual content and then approved by all the co-authors.

Appendix A. Supplementary dataset

577

578 The full data set is provided as Balagizietal_dataset1 XLS file.

579

580 **Appendix B. Supporting information Fig. S1**

References

Aoki K., T. Yoshida, K. Yusa, and Y. Nakamura., 1985. Petrology and geochemistry of the Nyamuragira volcano, Zaire, J. Volcanol. Geotherm. Res 25, 1-28.

Balagizi C.M., G. Mavonga, M. Kasereka, M. Liotta, M. Manzo, R. Lanari, M. Bonano, C. De Luca, G. Onorato, J. Lukindula, G. Ganci, C. Del Negro, A. Cappello, M. Coltelli, M. Mattia, D. Coppola, R. J. Durrheim, P. Mukambilwa, A. Kyambikwa, N. Mashagiro, H. Ciraba, J. B. Lowenstern, P. J Kelly, W. McCausland, A. Kies; 2020. Virunga Volcanoes Supersite Biennial Report: 2017- 2019; DOI: 10.5281/zenodo.3910912; https://zenodo.org/record/3911065#.XxHxQ54zY2w

Balagizi M.C. and M. Liotta, 2019. Key factors of precipitation stable isotope fractionation in Central-Eastern Africa and Central Mediterranean. Geosciences 2019, 9, 337 https://www.mdpi.com/2076-3263/9/8/337

Balagizi C.M., M. Kasereka, E. Cuoco, M. Liotta, 2019. Environmental and health impacts of Nyiragongo and Nyamulagira Volcanoes, East Africa. Geophysical Research Proceeding 2019, Vol. 21, EGU2019-5695. https://meetingorganizer.copernicus.org/EGU2019/EGU2019-5695.pdf

Balagizi, M.C, M.M. Kasereka, E. Cuoco, M. Liotta, 2018a. Influence of moisture source dynamics and weather patterns on stable isotopes ratios of precipitation in Central Eastern Africa. Science of the Total Environment Journal, 628 (629C), 1058-1078, https://doi.org/10.1016/j.scitotenv.2018.01.284

Balagizi, M.C, A. Kies, M. M. Kasereka, D. Tedesco, M. M. Yalire, W. A. McCausland., 2018b. Natural hazards in Goma and the surrounding villages, East African Rift System. Springer's Journal of Natural Hazards, 93, 31–66, https://doi.org/10.1007/s11069-018-3288-x

Balagizi M. C., M. M. Kasereka, E. Cuoco, M. Liotta, 2017. Rain-plume interactions at Nyiragongo and Nyamulagira volcanoes and associated rainwater hazards, East Africa, Applied Geochemistry 81 (2017) 76-89 ; http://dx.doi.org/10.1016/j.apgeochem.2017.03.018

Balagizi, M.C., M. M. Yalire, H. M. Ciraba, V. B. Kajeje, A. S. Minani, A. B. Kinja, M. M. Kasereka, 2016. Soil temperature and CO_2 degassing, SO_2 fluxes and field observations before and after the February 29, 2016 new vent inside Nyiragongo crater. Bulletin of Volcanology, 78 (9):1-11, https://link.springer.com/article/10.1007/s00445-016-1055-y

Balagizi, M.C., F. Darchambeau, M. Yalire, S. Bouillon, and Borges, A.V (2015), River geochemistry, chemical weathering, and atmospheric CO2 consumption rates in the Virunga Volcanic Province (East Africa), Geochem. Geophys. Geosyst., 16, 2637–2660, doi:10.1002/2015GC005999

Coppola D., Campion R., Laiolo M., Cuoco E., Charles M. Balagizi, Ripepe M., Cigolini C., Tedesco D., 2016. Birth of a lava lake: Nyamulagira volcano 2012-2015, Bulletin of volcanology, 78:20, https://link.springer.com/article/10.1007/s00445-016-1014-7

627

628 Craig H., 1963. The isotope geochemistry of water and carbon in geothermal areas. Nuclear
629 Geology in Geothermal Areas (E. Tongiorgi, ed.) Lab. Di Geologia Nucleare, Pisa., 17-53

630

631 Craig H., 1961. Isotopic variations in meteoric waters. Science, 133 (3465), 1702-1703. DOI:
632 10.1126/science.133.3465.1702

633 Cuoco E., A. Spagnuolo, C.M. Balagizi, F. De Francesco, F. Tassi, O. Vaselli, D.Tedesco,
634 2013a. Impact of volcanic emissions on rainwater chemistry: the case of Mt. Nyiragongo in the
635 Virunga volcanic region (DRC). J. Geochem. Explor.125, 69-79.
636 http://dx.doi.org/10.1016/j.gexplo.2012.11.008.

637

638 Cuoco E., D. Tedesco, R.J. Poreda, J.C. Williams, S. De Francesco, C.M. Balagizi, T.H. Darrah,
639 2013b. Impact of volcanic plume emissions on rain water chemistry during the January 2010
640 Nyamuragira eruptive event: Implications for essential potable water resources. J. Hazard. Mater.
641 244-245, 570-581. http://dx.doi.org/10.1016/j.jhazmat.2012.10.055.

642

643 Dansgaard, W.,1964. Stable isotopes in precipitation. Tellus. 16,438-468

644

645 De Mulder M. and P. Pasteels,1986. K-Ar geochronology of the Karisimbi volcano (Virunga,
646 Rwanda - Zaire). J. Afr. Earth Sci. 5, 575e579

Dewalle D. R., P. J. Edwards, B. R. Swistock, R. Aravena, and R. J. Drimmies, 1997. Seasonal isotope hydrology of three Appalachian forest catchments, Hydrological Processes, vol. 11, 1895-1906

DeWalle, D. R. and B. R. Swistock, 1994. Differences in oxygen-18 content of throughfall and rainfall in hardwood and coniferous forests, Hydrol. Process., 8, 75-82

Ebinger, C., 1989. Tectonic development of the western branch of the East African Rift System. Geol. Soc. Am. Bull., 101, 885-903.

Fisher, T.P. and G. Chiodini., 2015. Volcanic, Magmatic and Hydrothermal gases, In The Encyclopedia of Volcanoes, Second Edition, (H. Sigurdsson, B. Houghton, S. McNutt, H. Rymer and J. Stix, Edts), Elsevier, 779-798, ISBN: 978-0-12-385938-9

Gat J. R.2010. Isotope Hydrology: A Study of the Water Cycle, Imperial College Press, London, 197p

Gat J. R., 1996. Annual Review of Earth and Planetary Sciences, 24(1), 225–262. doi:10.1146/annurev.earth.24.1.225

667 Genereux D.P. and R.P. Hooper, 1998. Oxygen and hydrogen isotopes in rainfall–runoff studies,
668 in (Kendall, C. and J.J. McDonnell, Eds) Isotope tracers in catchment hydrology, Elsevier
669 Science, Amsterdam 319–346

670

671 Geyh, M.A., 2005. Dating of old groundwater-History, potential, limits and future, in Isotopes in
672 the water cycle: past, present and future of a developing science, Aggarwal P., J.R.
673

674 Head E. M., Carn S. A., Sims K. W., Shaw A. M., Wallace P. J., Maclean A., 2009. Degassing
675 from a Mafic Alkaline Shield Volcano: Nyamulagira, D.R. Congo. American Geophysical
676 Union, Fall Meeting 2009, abstract #V13E-2070. Code: 2009AGUFM.V13E2070H
677

678 Hoefs, J. (2009), Stable Isotope Geochemistry Sixth Edition, Springer, Verlag-Berlin-
679 Heidelberg, 293 p; doi: 10.1007/978-3-540-70708-0

680

681 Holland, D. and K. K. Turekian., 2010. Isotope Geochemistry: A derivative of the Treatise on
682 Geochemistry, Academic Press, United Kingdom, 752 p

683

684 Huang T.M., Pang Z.H., 2012. The role of deuterium excess in determining the water salinisation
685 mechanism: a case study of the arid Tarim River Basin, NWChina. Appl Geochem 27(12):2382–
686 2388

687

688 IAEA/WMO, 2017. Global Network of Isotopes in Precipitation. The GNIP Database. Available
689 at. http://www.iaea.org/water

690

691 Kendall C., 1993. Impact of Isotopic Heterogeneity in Shallow Systems on Stormflow
692 Generation, Ph.D. dissertation, University of Maryland, College Park, 310 p.

693

694 Komorowski, J.-C.; Tedesco, D.; Kasereka M.C.; Allard P.; Papale, P.; Vaselli, O.; Durieux ,J.;
695 Baxter, P.; Halbwachs, M.; Akumbi, M.; Baluku, B.; Briole, P.; Ciraba, M.; Dupin, J.-C.; Etoy,
696 O.; Garcin, D.; Hamaguchi, H.; Houlié, N.; Kavotha, K.S.; Lemarchand, A.; Lockwood, J.;
697 Lukaya, N.; Mavonga, G.; de Michele, M.; Mpore, S.; Mukambilwa, K.; Munyololo, F.;
698 Newhall, C.; Ruch ,J.; Yalire M.M.; Wafula, M., 2004. The January 2002 flank eruption of
699 Nyiragongo volcano (Democratic Republic of Congo): Chronology, evidence for a tectonic rift
700 trigger, and impact of lava flows on the city of Goma. Acta Vulcanol. 15 (1-2), 27–62

701

702 Levin, N. E., E. J. Zipser, and T. E. Cerling., 2009. Isotopic composition of waters from Ethiopia
703 and Kenya: Insights into moisture sources for eastern Africa, J. Geophys. Res., 114, D23306,
704 doi:10.1029/2009JD012166

705

706 Liu K., Qiao, X., Li, B. et al., 2016. Characteristics of deuterium excess parameters for
707 geothermal water in Beijing. Environ Earth Sci 75, 1485. https://doi.org/10.1007/s12665-016-
708 6285-y

Mduma N.P., Komakech, H.C., Zhang, J.,Muzuka, A.N.N., 2016. Application of isotopes and water balance on Lake Duluti–groundwater interaction, Arusha, Tanzania of isotopes and water balance on lake duluti-groundwater interaction, Arusha, Tanzania. Hydrol. Earth Syst. Sci. Discuss. https://doi.org/10.5194/hess-2016-176

Merkel B. J. and B. Planer-Friedrich. 2002, Groundwater Geochemistry: A Practical Guide to Modeling of Natural and Contaminated Aquatic Systems. Translated and updated fromthe German version "Grundwasserchemie", Springer, Verlag-Berlin-Heidelberg, Germany.

Mironenko, M.V. and Zolotov, M. Y., 2012. Equilibrium–Kinetic Model of Water–Rock Interaction. Geokhimiya, 50 (1), 3–9. https://doi.org/10.1134/S0016702912010089

Munyaneza O., Wenninger, J., Uhlenbrook, S., 2012. Identification of runoff generation processes using hydrometric and tracer methods in a meso-scale catchment in Rwanda. Hydrol. Earth Syst. Sci. 16 (7):1991–2004. https://doi.org/10.5194/hess-16-1991-2012

Muvundja A. F., A. Wüest, M. Isumbisho, M. Kaningini, N. Pasche, P. Rinta, M. Schmid, 2014. Modelling Lake Kivu water level variations over the last seven decades, Limnologica-Ecology and Management of Inland Waters 47, 21-33, doi:10.1016/j.limno.2014.02.003

729 Pfahl, S. and H. Sodemann (2014), What controls deuterium excess in global precipitation?,
730 Clim. Past, 10, 771–781, doi:10.5194/cp-10-771-2014

731

732 Platz, T., S. F. Foley, and L. Andre., 2004. Low-pressure fractionation of the Nyiragongo
733 volcanic rocks, Virunga Province, D.R. Congo, J. Volcanol. Geotherm. Res. 2004;136:269–295,
734 doi:10.1016/j.jvolgeores.2004.05.020.

735

736 Prasetio R., Z. Abidin1, and Y. Yulizar., 2010. Isotope and Gas Geochemistry of Dieng
737 Geothermal Field, Indonesia, Proceedings World Geothermal Congress 2010, Bali, Indonesia,
738 25-29 April 2010.

739

740 Pouclet A. and K. Bram, 2021. Nyiragongo and Nyamuragira: a review of volcanic activity in
741 the Kivu rift, western branch of the East African Rift System. Bull Volcanol 83, 10.
742 https://doi.org/10.1007/s00445-021-01435-6

743

744 Purnomo B. J. and T. Pichler., 2014. Geothermal systems on the island of Java, Indonesia,
745 Journal of Volcanology and Geothermal Research 285, 47-59, doi:
746 10.1016/j.jvolgeores.2014.08.004

747 Rozanski, K., 1985. Deuterium and oxygen-18 in European groundwaters – links to atmospheric
748 circulation in the past. Chem. Geol. 52, 349–363.

749 Rozanski, K., Araguaś-Araguaś, L., Gonfiantini, R., 1993. Isotopic patterns inmodern global
750 precipitation. In: Swart, P.K., Lohmann, K.C., Mckenzie, J., Savin, S. (Eds.), Climate Change in

751 Continental Isotopic Records. 78. American Geophysical Union: pp.1–35.
752 https://doi.org/10.1029/GM078p0001.
753
754 Trabucco A. R.J. Zomer, 2009. Global Aridity Index (Global-Aridity) and Global Potential
755 Evapotranspiration (Global-PET) Geospatial Database. CGIAR Consortium for Spatial
756 Information. (Published online, available from the CGIAR-CSI GeoPortal at).
757 http://www.csi.cgiar.org
758
759 Villeneuve, M., 1980. La structure du Rift Africain dans la R´egion du Lac Kivu (Za¨ıre
760 oriental), B. Volcanol., 43–3, 541–551, doi:10.1007/BF02597691.
761
762 Wassenaar L. I., T. B Coplen, and K. A. Pradeep., 2014. Approaches for Achieving Long-Term
763 Accuracy and Precision of δ18O and δ2H for Waters Analyzed using Laser Absorption
764 Spectrometers, Sci. Technol., 48, 1123-1131, dx.doi.org/10.1021/es403354n
765
766 Wauthier, C., Cayol, V., Kervyn, F., d'Oreye, N. (2012), Magma sources involved in the 2002
767 Nyiragongo eruption, as inferred from an InSAR analysis. J. Geophys. Res. 117 (B05411), 1-20
768
769 Yin G. and Ni SJ., 2001. Deuterium excess parameter evolution in ground water. Bull of Mineral
770 Petrol Geochem 20(4):409–411
771
772 Zomer R.J., D.A. Trabucco Bossio, O. van Straaten, L.V. Verchot 2008. Climate change
773 mitigation: a spatial analysis of global land suitability for clean development mechanism
774 afforestation and reforestation. Agric. Ecosyst. Environ. 126, 67–80.

775

776 Zomer R.J., Bossio D.A., Trabucco A., Yuanjie L., Gupta D.C., Singh V.P., 2007. Trees and
777 Water: Smallholder Agroforestry on Irrigated Lands in Northern India. International
778 WaterManagement Institute, Colombo, Sri Lanka, p. 45 (IWMI Research Report 122).

Figures

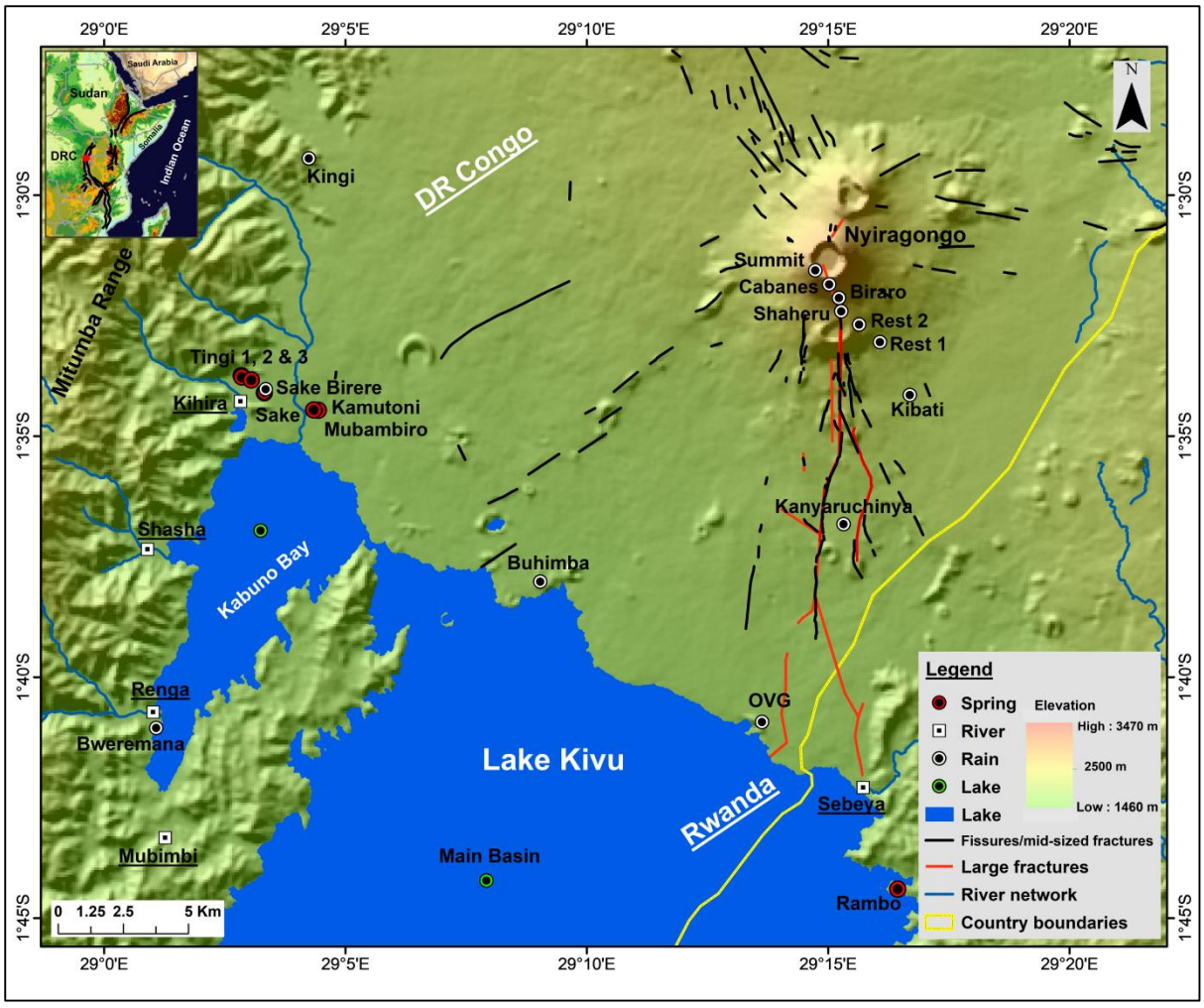

Figure 1. Topographical map of the north basin of Lake Kivu situated within the western branch of the East African Rift (shown in the inset map), on the border between the Democratic Republic of the Congo and the Republic of Rwanda. In the Sake area are found the following sampling sites: the Sake rain gauge; the Tingi springs group (1 to 3), Sake Birere spring, Kamutoni and Mubambiro springs.

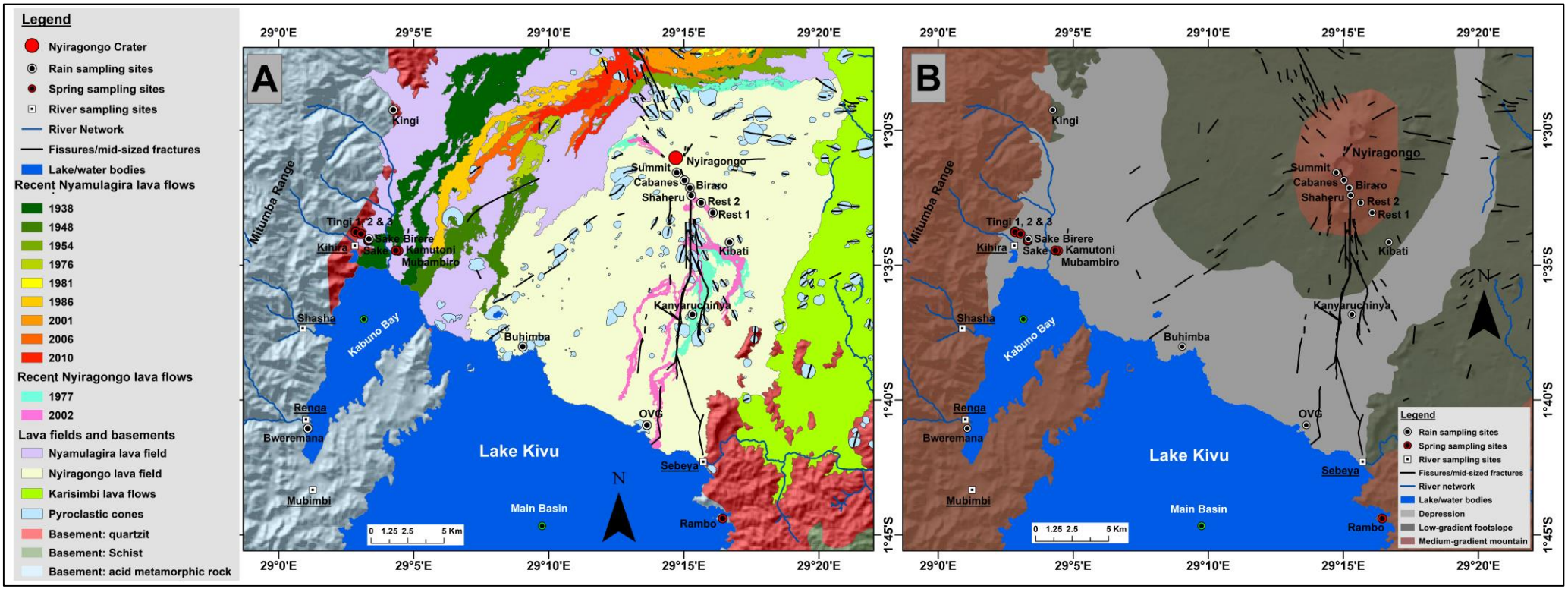

Figure 2. Maps of the lithology (A; from combined field observations and data from Balagizi et al. 2018b and Hartmann and Moosdorf, 2012) and of the landforms (B; including depression, upper footslope and medium to high gradient-mountains) in the north basin of Lake Kivu located in the western branch of the East African Rift, on the border between the Democratic Republic of the Congo and the Republic of Rwanda.

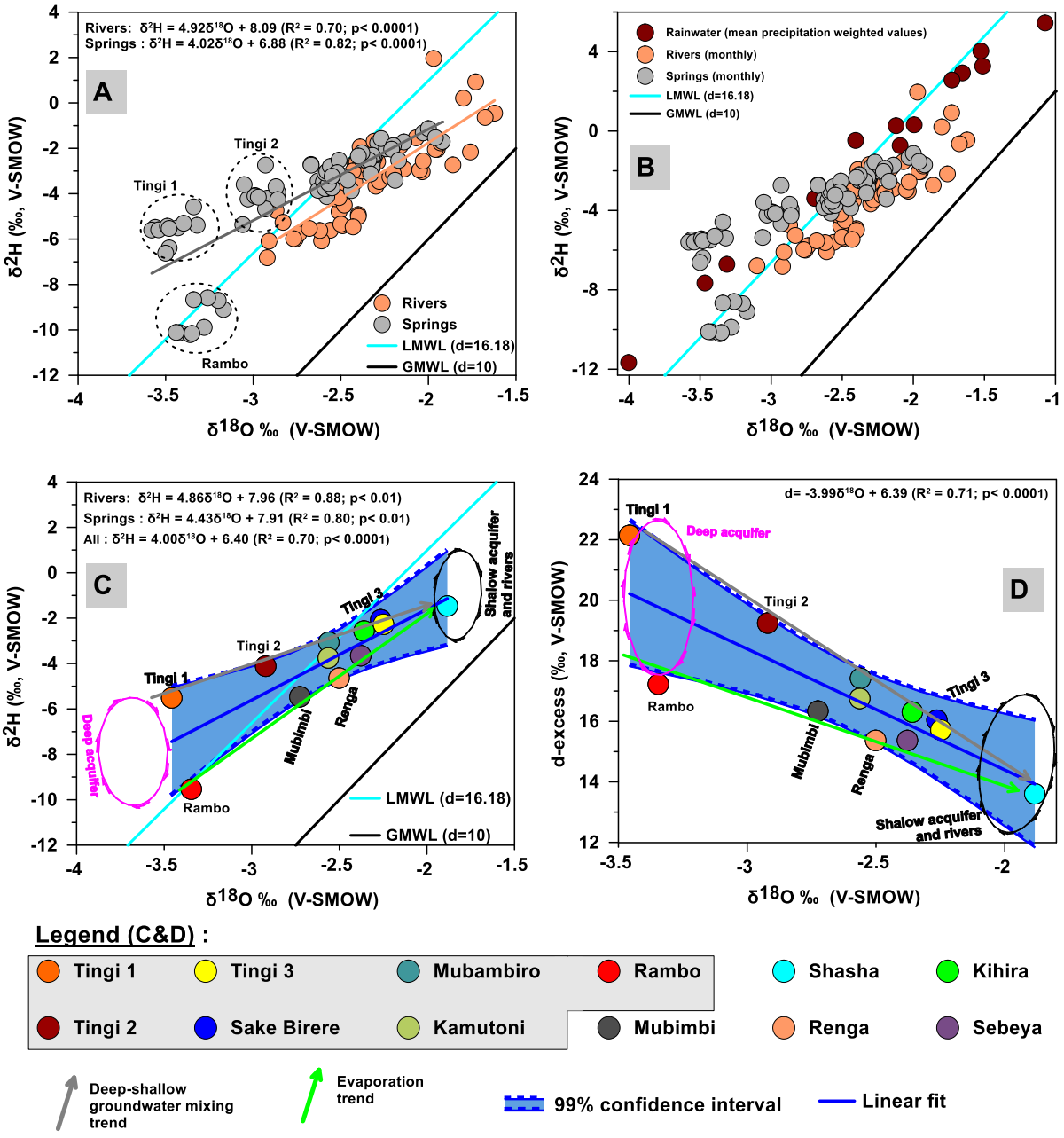

Figure 3. Plots of monthly δ^2H versus $\delta^{18}O$ of rivers and springs (A); of monthly δ^2H versus $\delta^{18}O$ of rivers and springs where mean precipitation-weighed values of precipitation are added (B); and of mean δ^2H versus $\delta^{18}O$ of springs (with grey background in the legend for figures C&D) and rivers (C&D). Rivers and springs samples were collected between November 2013 and October 2014, while precipitation were collected between December 2013 and October 2015 in the north catchment of Lake Kivu. The LMWL refers to the Local Meteoric Water Line of equation $\delta^2H=7.60\delta^{18}O +16.18$ after Balagizi et al, 2018a, and the

GMWL to the Global Meteoric Water Line of equation $\delta^2H=8\delta^{18}O+10$ after Craig, 1961 and Rozanski et al., 1993.

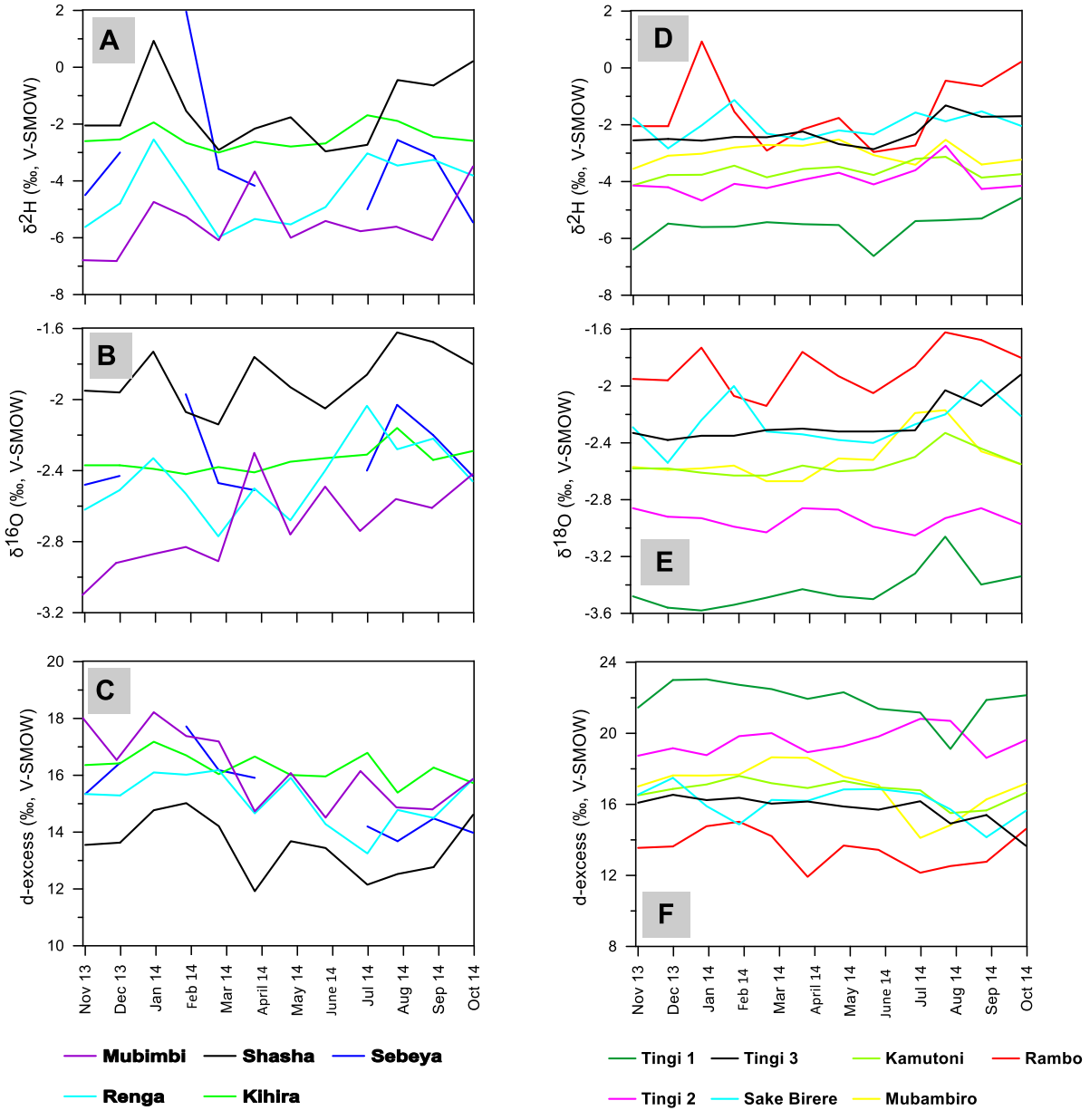

Figure 4. Temporal evolution of monthly δ^2H (A and D), $\delta^{18}O$ (B and E) and deuterium excess (C and F) in rivers (A, B and C) and springs (D, E and F) sampled on monthly basis between November 2013 and October 2014 in the north catchment of Lake Kivu, eastern Democratic of the Congo.

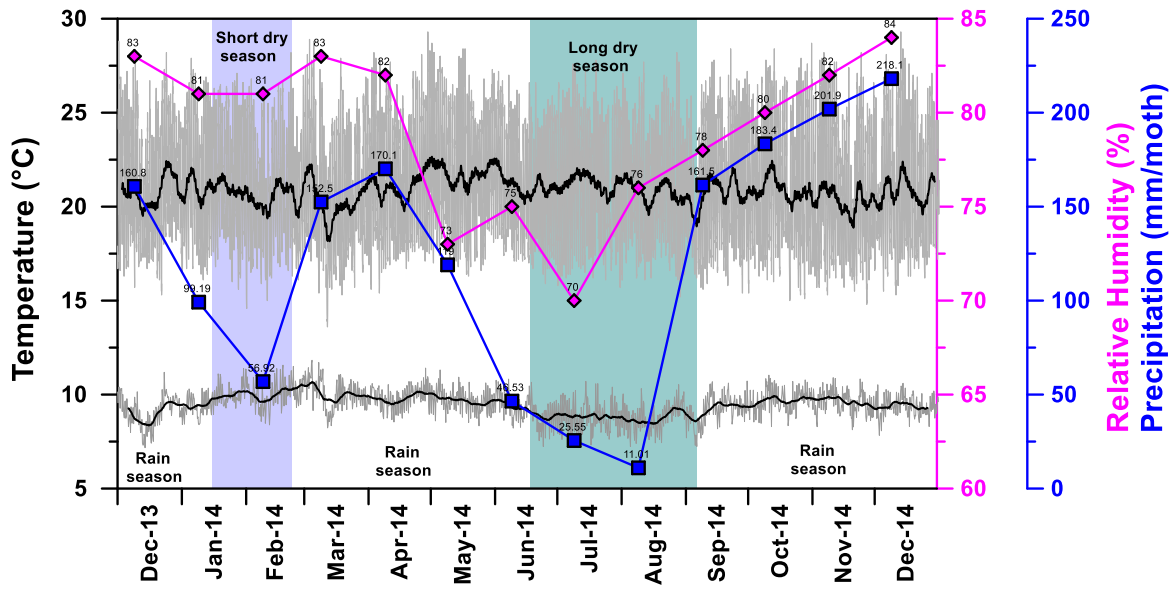

Figure 5. Temporal evolution of air temperature, precipitation and air relative humidity between December 2013 and December 2014 in Goma city; eastern Democratic Republic of the Congo and the Republic. The grey upper and lower lines are respectively daily data collected on 30 minutes interval by a Davis Vantage Pro2 weather station based in Goma city, and 6 hours intervals by the ERA-Interim model of the European Centre for Medium-Range Weather Forecast (ECMWF) at the summit of Nyiragongo (at 700 mbar). The black lines are running averages of the daily temperature. Relative humidity are daily means obtained from data collected on 30 minutes interval by the Davis Vantage Pro2 weather in Goma city. The monthly precipitation is deduced from the volume of monthly rainwater recorded in a rain-gauge installed at Bweremana (Fig. 1).

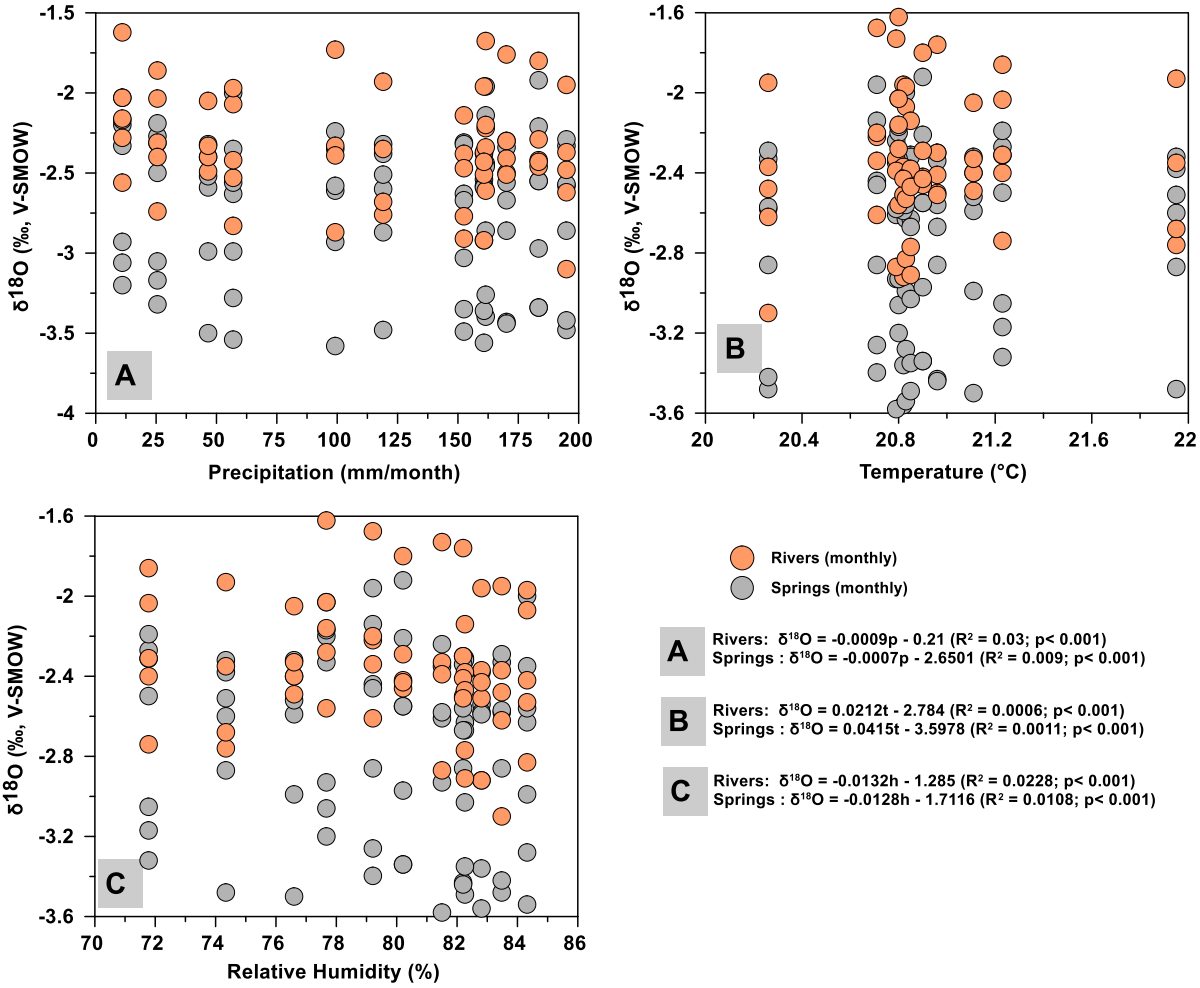

Figure 6. Plot of monthly $\delta^{18}O$ from rivers and springs versus monthly precipitation (A), daily mean temperature (B) and daily mean relative humidity (C). Oxygen stable isotope data is from water samples collected monthly in rivers and springs of the north basin of Lake Kivu in eastern Democratic of the Congo, between December 2013 and December 2014. Daily air temperature and relative humidity are arithmetic means obtained from data collected on 30 minutes interval by a Davis Vantage Pro2 weather station in Goma city.

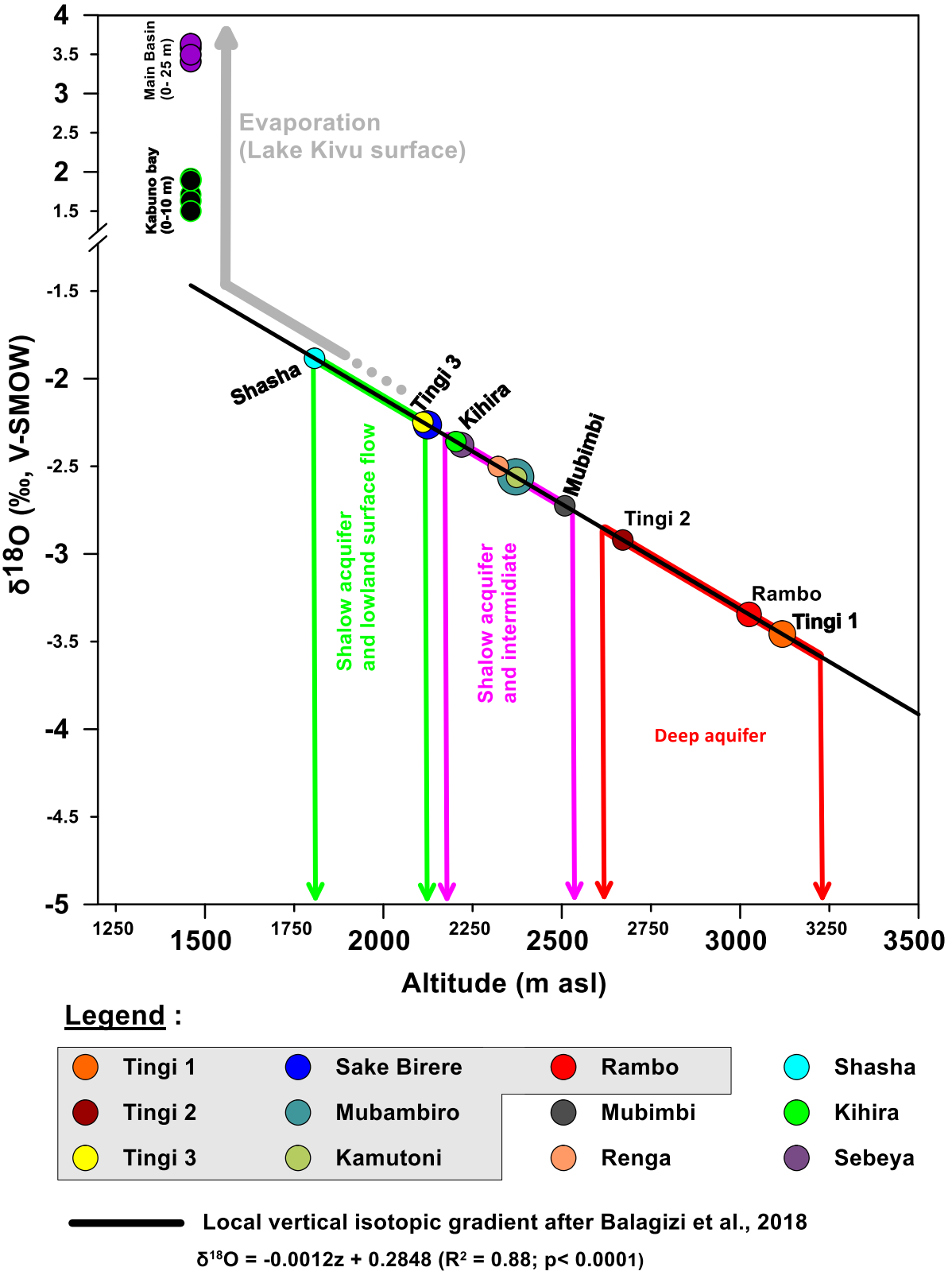

Figure 7. Plot of mean precipitation-weighted $\delta^{18}O$ of springs (with grey background in the legend) and rivers versus the altitude. Lake Kivu $\delta^{18}O$ data is from water samples collected from the lake's upper layer (0 and 25 m in the Main Basin; 0,5 and 10 m in the Kabuno Bay; Fig. 1 andTable 2). The solid black line displays the local vertical $\delta^{18}O$ gradient line of

equation $\delta^{18}O = - 0.0012z + 0.2848$ after Balagizi at all., 2018a; which was obtained using mean precipitation-weighted $\delta^{18}O$ values. The grey solid line indicates the water transfer from rivers to Lake Kivu and the evaporation taking place over the lake's surface.

Tables

Table 1. Min-arithmetic mean-max of temperature (°C), precipitation (mm), δ^2H, $\delta^{18}O$ and deuterium excess (‰) of rivers and springs water collected on monthly basis in the north basin of Lake Kivu, eastern Democratic Republic of the Congo and north-western Rwanda, between November 2013 and December 2014

Site name	Type	Elevation (m a.s.l.)	Temperature (°C)			Precipitation[a] (mm)			δ^2H (‰)			$\delta^{18}O$ (‰)			d-excess (‰)			Number of samples
			Min	Mean	Max	Min	Mean	Max	Min	Mean	Max	Min	Mean	Max	Min	Mean	Max	
Mubimbi	**River**	1506	17.40	18.78	20.70	9.87	110.80	218.11	-6.82	-5.48	-3.49	-3.10	-2.71	-2.30	14.51	16.20	18.22	12
Renga	**River**	1471	20.00	21.85	24.30	9.87	110.80	218.11	-5.98	-4.38	-2.54	-2.77	-2.44	-2.04	13.25	15.18	16.18	12
Shasha	**River**	1472	21.10	24.23	26.90	9.87	110.80	218.11	-2.96	-1.51	0.93	-2.14	-1.88	-1.62	11.92	13.52	15.02	12
Kihira	**River**	1469	19.60	20.60	21.70	4.26	107.49	206.47	-3.00	-2.45	-1.69	-2.42	-2.34	-2.16	15.39	16.29	17.18	12
Sebeya	**River**	1475	20.35	20.79	21.23	7.27	104.51	214.78	-5.46	-3.27	1.96	-2.51	-2.32	-1.97	13.68	15.33	17.72	9
Tingi 1	**Tepid spring**	1493	29.00	29.32	29.54	4.26	107.49	206.47	-6.62	-5.56	-4.58	-3.58	-3.43	-3.06	19.12	21.89	23.04	12
Tingi 2	**Tepid spring**	1498	26.20	26.56	26.90	4.26	107.49	206.47	-4.67	-3.98	-2.74	-3.05	-2.94	-2.86	18.62	19.53	20.82	12
Tingi 3	**Cold spring**	1501	21.60	21.70	21.81	4.26	107.49	206.47	-2.86	-2.28	-1.32	-2.38	-2.26	-1.92	13.67	15.77	16.54	12
Sake Birere	**Cold spring**	1475	18.10	18.22	18.30	4.26	107.49	206.47	-2.83	-2.01	-1.13	-2.54	-2.26	-1.96	14.15	16.09	17.49	12
Kamutoni	**Cold spring**	1492	17.39	17.41	17.43	4.26	107.49	206.47	-4.13	-3.64	-3.13	-2.63	-2.55	-2.33	15.51	16.76	17.60	12
Mubambiro	**Cold spring**	1496	17.40	17.41	17.44	4.26	107.49	206.47	-3.55	-3.01	-2.52	-2.67	-2.50	-2.17	14.11	17.02	18.65	12
Rambo	**Hot spring**	1461	72.30	72.72	73.20	7.27	104.51	214.78	-10.21	-9.50	-8.59	-3.44	-3.31	-3.17	16.26	17.00	18.05	9

[a] The precipitation data used for Mubimbi, Renga and Shasha rivers are from a station located at Bweremana (1470 m a.s.l.), precipitation data for Kihira river, Tingi 1 & 2 tepid springs, Tingi 3, Sake Birere, Kamutoni and Mubambiro cold spring are from a station located at Sake (1514 m a.s.l.) while the precipitation data for Sebeya river and Rambo hot spring are from OVG station (1535 m a.s.l.). Refer to the map of **Fig. 1** to locate these stations in the study area.

Table 2. Min-arithmetic mean-max precipitation (mm), min-arithmetic mean-max δ^2H, $\delta^{18}O$ and deuterium excess (‰) of precipitation and the corresponding mean precipitation weighted values, and δ^2H, $\delta^{18}O$ and deuterium excess (‰) of the 25 m upper layer of Lake Kivu; collected in the north basin of Lake Kivu, eastern Democratic Republic of the Congo, between December 2013 and October 2015.

	Elevation (m a.s.l.)	Precipitation[b] (mm)			δ^2H (‰)			$\delta^{18}O$ (‰)			d-excess (‰)			Mean precipitation weighted values			Number of samples
		Min	Mean	Max	Min	Mean	Max	Min	Mean	Max	Min	Mean	Max	δ^2H (‰)	$\delta^{18}O$ (‰)	d (‰)	
Bweremana (lowland site)	1470	9.87	110.80	218.11	-12.22	10.84	58.89	-3.42	-0.27	5.98	-3.58	13.02	20.20	5.45	-1.07	14.03	23
Sake (lowland site)	1514	4.26	107.49	206.47	-18.10	8.95	41.74	-4.15	-0.81	4.04	5.54	15.40	19.69	3.28	-1.51	15.38	23
Kingi (lowland site)	1848	14.12	139.45	283.12	-17.91	3.30	29.46	-4.22	-1.62	1.44	13.42	16.25	19.20	0.31	-1.99	16.27	18
Buhimba (lowland site)	1468	5.71	119.87	223.61	-21.47	7.10	37.44	-4.74	-1.17	2.44	11.11	16.49	20.49	2.93	-1.65	16.16	20
OVG (lowland site)	1535	7.27	104.51	214.78	-17.73	4.54	32.87	-3.99	-1.38	2.51	6.47	15.54	20.37	-0.74	-2.09	16.01	21
Kanyaruchinya (lowland site)	1759	7.48	139.32	320.30	-18.47	8.91	56.02	-4.60	-0.89	6.16	6.74	16.00	22.03	4.03	-1.53	16.23	22
Kibati (lowland site)	1994	5.40	143.74	263.80	-23.70	5.29	34.11	-4.87	-1.41	1.86	11.24	16.60	19.48	2.57	-1.73	16.40	22
Rest 1 (highland site)	2254	12.05	194.11	372.44	-24.61	4.41	46.80	-4.91	-1.63	3.66	14.69	17.42	20.82	0.27	-2.12	17.24	14
Rest 2 (highland site)	2535	15.37	188.31	376.60	-25.84	0.90	41.50	-5.42	-2.19	2.49	15.92	18.40	21.58	-3.39	-2.69	18.16	14
Shaheru (highland site)	2761	53.18	176.36	339.21	-27.27	2.99	39.75	-5.66	-2.01	2.53	17.41	19.08	20.86	-0.47	-2.41	18.78	12
Biraro (highland site)	2918	35.73	194.35	357.28	-30.54	-2.02	34.51	-5.99	-2.76	1.66	17.37	20.06	21.83	-6.71	-3.31	19.78	12
Cabanes (highland site)	3230	47.98	177.01	339.00	-32.30	-3.73	29.08	-6.36	-3.01	0.95	18.56	20.38	23.48	-7.66	-3.47	20.07	12
Summit (highland site)	3460	23.26	174.60	274.40	-32.53	-7.19	32.64	-6.44	-3.50	1.28	18.74	20.78	22.92	-11.66	-4.00	20.36	10
Kabuno Bay (0 m depth)	1460	—	—	—	17.99	18.70	19.36	1.71	1.84	1.92	3.55	3.96	4.31	—	—	—	3
Kabuno Bay (5 m depth)	1460	—	—	—	17.64	18.15	18.66	1.63	1.76	1.89	3.54	4.07	3.54	—	—	—	2
Kabuno Bay (10 m depth)	1460	—	—	—	—	17.45	—	—	1.50	—	—	5.45	—	—	—	—	1
Kivu Main Basin (0 m depth)	1460	—	—	—	26.22	26.99	27.76	3.41	3.49	3.58	-2.42	-0.96	0.50	—	—	—	2
Kivu Main Basin (25 m depth	1460	—	—	—	26.05	26.69	27.33	3.50	3.56	3.63	-3.02	-1.83	-0.63	—	—	—	2